Article

Integrating Highly Efficient Recognition and Signal Transition of g-C3N4 Embellished Ti3C2 MXene Hybrid Nanosheets for Electrogenerated Chemiluminescence Analysis of Protein Kinase Activity

Yan Sun, Yimeng Zhang, Huixin Zhang, Meiling Liu, and Yang Liu

Anal. Chem., **Just Accepted Manuscript** • DOI: 10.1021/acs.analchem.0c01776 • Publication Date (Web): 30 Jun 2020

Integrating Highly Efficient Recognition and Signal Transition of g-C_3N_4 Embellished Ti_3C_2 MXene Hybrid Nanosheets for Electrogenerated Chemiluminescence Analysis of Protein Kinase Activity

Yan Sun,[†,‡] Yimeng Zhang,[‡] HuiXin Zhang,[‡] Meiling Liu,[*,†] Yang Liu[*,‡]

[†]Key Laboratory of Chemical Biology & Traditional Chinese Medicine Research (Ministry of Education, China), College of Chemistry and Chemical Engineering, Hunan Normal University, Changsha 410081, P. R. China

[‡]Department of Chemistry, Beijing Key Laboratory for Analytical Methods and Instrumentation, Key Laboratory of Bioorganic Phosphorus Chemistry & Chemical Biology of Ministry of Education, Tsinghua University, Beijing 100084, China

* Corresponding author

E-mail address: liumeilingww@126.com, liu-yang@mail.tsinghua.edu.cn

ABSTRACT

Herein, a novel electrogenerated chemiluminescence (ECL) method for highly sensitive kinase activity and inhibitors screening were developed based on a graphitic carbon nitride nanosheet (g-C_3N_4) nanoparticles embellished titanium carbide (Ti_3C_2) MXenes nanosheets, integrating the highly efficient recognition and signal amplification. activity. In this strategy, kemptide was first immobilized onto a gold electrode, and it was phosphorylated by the protein kinase A which used as a model. The g-C_3N_4-MXenes probe can adsorbed explicitly onto the electrode based on chelation between the phosphate group and Ti defect sites enriched in MXenes. Besides the abundant active sites on MXene for the highly efficient binding with phosphate groups, the Ti_3C_2 MXene do not only provide a unique conductive platform to accommodate more g-C_3N_4 nanoparticles but also facilitate the electron transfer on the electrode interface and suppress the passivation of g-C_3N_4 that explores their highly efficient ECL emission with high stability. The obtained ECL signals was closely related to the kinase activity and can be applied for PKA activity detection. Under the optimal conditions, the proposed ECL biosensor provided a quantitative readout to PKA concentration in the range of 0.015-40 U mL^{-1} with the detection limit of 1.0 mU mL^{-1}. The ECL biosensor was also successfully applied to monitor drug-triggered kinase activation and quantitative analysis of the kinase inhibitors in MCF-7 cell lysates. This work presents that the proposed ECL biosensor has the potential to be a powerful tool for PKA study and clinical diagnostics as well as the discovery of new targeted drugs.

Keywords: Electrochemiluminescence; MXenes; protein kinase A (PKA); electron transfer; g-C_3N_4-MXenes

INTRODUCTION

Due to the primary roles in cell growth, division, differentiation, adhesion, motility and death, protein kinases have become major drug targets against human diseases such as heart failure[1] and cancer,[2] which regulate various aspect of cellular activity that mediate the development and regulation of both unicellular and multicellular organisms. As a necessary post-translational modification, the phosphorylation of proteins plays a pivotal role in signal transduction and cellular regulation.[3] Protein kinase has been used as one of the important biomarkers for the diagnosis of diseases, it is essential for a deep understanding of the basic biochemical processes of signal transduction. Over-expression of protein kinases is closely associated with multiple diseases and the aberrant activities of protein kinases are related to many diseases such as cancer[4], Alzheimer's disease[5], inflammation, diabetes, cardiovascular diseases[6], central nervous system disorder[7] and so on. Besides, kinase inhibitors can regulate down the activity of related protein kinases and have been investigated as effective drugs for cancer therapies, and the screening of kinase inhibitors are importance in medicinal researches and clinical treatments[8]. Therefore, accurate determination of protein kinase activity and its potential inhibitors screening are beneficial to the development of protein kinase-targeted drugs and molecular targeted therapy.

The conventional methods for PKA detection are based on the radiolabeling of substrate peptides with ^{32}P in the presence of γ-^{32}P-ATP as the phosphate group donor.[14] However, most methods suffer from certain drawbacks, such as expensive and harmful radioactive labels, complex instruments or complex operation. The colorimetric,[9] electrochemical,[10,11] fluorescent[12,13] based immunoassays approaches have been recently reported as the alternative ways for the protein kinase activity analysis and inhibitor screening by the usage of labeled phosphor-specific antibodies. The high affinity of antibody-antigen improves the selectivity of biosensors.[4,21] However, these immunoassays generally suffered the false positive analysis, poor storage stability and crosslink reaction from the intrinsic immunoreactions. Recently, Electrogenerated chemiluminescence have received much attention, which is a light emission process in a redox reaction of electrogenerated reactants, and combines the advantages of the

electrochemistry and luminescence with high sensitivity, [15] simple instrument, [16] easy miniaturization[17] and low cost. [18] What's more, the ECL technique is potential and spatial controlling, and is potential in the high throughput analysis.[19] Recently, an ECL based immunosensor for the kinase activity has been reported with wide linear range.[8] In addition, the ECL biosensor for multiple kinase activity detection were also developed using a ruthenium-labeled protein A as an ECL probe which could bind to the Fc region of a variety of antibodies with high affinity.[20] However, most of these methods are involved the employment of biorecognition units such as antibody and protein A and so on, which are limited in the storage stability, sensitivity and the false positive analysis from the crosslink immunoreactions, and it is difficult to be explored for the analysis of uncertain kinase. As an alternative way, the ECL biosensors were also designed using thiol-adenosine triphosphate as the coreactor, in which the thiophosphate group on the kemptide substrate after phosphorylation can specifically adsorb onto gold nanoparticles. This not only prevents false positive immunity, but also brings the ECL biosensors with high sensitivity owing to the excellent conductivity and catalytic activity of gold nanoparticles.[22,23] To avoid the usage of sulfhydryl compounds, an ECL biosensor was also fabricated using gold nanoparticles functionalized with phosphorylated DNA as probes which can specifically adsorbed with the phosphorylated peptide substrate by adding Zr^{4+} ions.[24] Nevertheless, the complicated assembly procedures limits their applications. Recently, a metal-organic framework (MOF) of UiO-66 encapsulated with $Ru(bpy)_3^{2+}$ were also applied for the design of ECL biosensor for kinase activity based on the chelation between the Zr^{4+} defects on the surface of UiO-66 and the phosphorylated peptide,[25] which avoids the limited point-to-point recognition of between the phosphate group with Zr^{4+} or antibody. While, the poor conductivity of MOF as well as the high background and toxicity of the coreactor of tripropylamine restrict the performances of these biosensors. Therefore, it is still a challenge to explore novel strategies and nanoprobes for the further improvement of sensitivity and accuracy of kinase activity analysis by integrating abundant active sites for the efficient recognition of phosphate group as well as the ECL signal transition.

Ti_3C_2 MXenes are a type of layered two-dimensional (2D) transition metal carbide

which own many excellent characters such as excellent electrical conductivity, extraordinary catalytic properties, low toxicity, large surface area,[27-31] and exhibit outstanding performance in sensing,[32] electronic devices,[33] catalysis fields[34-40] and energy storage materials[41,42]. Moreover, the physical and chemical performances of MXenes could also be improved by the size regulation, surface functionalization, and so on. For instance, the Ti sites were considered as the active sites for nitrogen reduction, the vertical orientation of MXene can expose more Ti active sites for electrocatalysis.[43] By depositing metallic nanoparticles on MXene, the ability of electrocatalytic activity and functionality can be further improved.[44] Up to now, MXenes have been applied for the detection of H_2O_2,[45] exosomes, [46] metal ions,[47] small organic molecules[48] etc. These unique features endow their great prospects in the establishment of biosensors.

In this work, a facile and novel ECL biosensor for highly sensitive detection of protein kinase A was constructed based on a MXenes hybrid nanoprobe(g-C_3N_4-MXenes) decorated with Graphitic-phase carbon nitrides, which are unique graphene-like carbon-based nanomaterials with highly efficient ECL emission, excellent biocompatibility and chemical stability.[26] In the presence of kinase, the kemptide was phosphorylated in the substrate of adenosine triphosphate (ATP). After phosphorylation, the hybrid nanoprobes, which enriched the recognition sites and integrated the highly efficient recognition and multiple signal amplification, could adsorbed onto the phosphorylated kemptide with high efficiency based on the chelation interaction between the Ti sites enriched in MXenes and phosphate groups. Moreover, the MXenes acted as the effective substrates to weaken the passivation of g-C_3N_4 and stabilized the ECL signals owing the large surface area and excellent conductivity, and thus generating strong and stable ECL signal. The ECL signal was enhanced with the increase of the kinase activity, and presented high sensitivity and selectivity to PKA detection. In addition, the quantitative kinase activities assay and inhibitors screening in complex cell lysates samples were also performed, which displayed great potential in clinic diagnosis and kinase-related life science researches.

EXPERIMENTAL SECTION

Materials and Reagents. Cysteine-terminated kemptide (CLRRASLG) was obtained from Sangon Biochem (Shanghai, China). Protein kinase A (PKA) was purchased from New England Biolabs, and adenosine 5-triphophate (ATP) was obtained from Solarbio Technologies Company (Beijing, China). 2,6,2′,6′-dilactone (ellagic acid), N-(3-chlorophenyl)-6,7-dimethoxy-4-quinazolinamine (Tyrphostin AG1478), epigallocatechin gallate (EGCG) were purchased from Solarbio Company, Forskolin and 3-isobutyl-1-methylxantine (IBMX) were purchased from Sigma. 6-mercapto-1-hexanol (MCH), polyetherimide (PEI) and $MgCl_2$ were purchased from Macklin. 1-(3-(dimethylamino) propyl)-3-ethylcarbodiimidehydrochloride (EDC) and N-hydroxysuccinimide sodium (NHS) were obtained from Alfa Aesar (Shanghai, China). Dulbecco's Modification of Eagle's Medium (DMEM) was purchased from Hyclone. Other reagents of analytical grade were supplied by Beijing Chemical Company (China). All solutions were prepared with deionized (DI) water.

Apparatus and characterization. The ECL measurements were carried out on an MPI-B multifunctional electrochemical analytical system (Xi'an Remex Analytical Instrument Ltd. Co., China) in the electrolyte of 20 mM $K_2S_2O_8$ and 0.1 M KCl. The voltage of photomultiplier tubes (PMT) was maintained at 600 V. The cyclic voltammetry was conducted on a CHI 660B instrument (CH Instrument Co.). The electrochemical cell was in a typical three-electrode system using the modified electrode as working electrode, platinum wire as counter electrode and Ag/AgCl, saturated KCl as reference electrode. Electrochemical impedance spectroscopy (EIS) was conducted on SP-150 (Bio-Logic, France) in 0.1 M KCl containing 5 mM of $K_3[Fe(CN)_6]/K_4[Fe(CN)_6]$ with the frequency range from 100 mHz to 100 kHz. Fourier transform infrared (FT-IR) spectra were obtained on a PerkinElmer Spectrum GX spectrometer (PerkinElmer Co., Waltham, MA). Ultrasonic pulverization was operated on Scientz-IID (SCIENTZ, China). Powder X-ray diffraction (XRD) analysis was obtained on a D8-Advance diffractometer (Cu Kα radiation, $\lambda = 0.15406$ nm, Bruker, Germany). A JSM7401 (JEOL, Japan) field emission scanning electron microscopy (SEM) system, H-7650B (HITACHI, Japan), transmission electron microscope (TEM), and high-resolution transmission electron microscope (HRTEM) images observed at

JEM 2100F (JEOL, Japan).

Synthesis of g-C_3N_4-MXenes Nanocomplex. Ti_3C_2 MXenes was obtained from the etching of Ti_3AlC_2 MAX powder (<38 μm particle size), and the synthesis method is similar to the literature,[49-51] as shown in Scheme 1A. Briefly, the preparation process of single layer MXenes was introduced: LiF (0.8 g) was slowly poured into HCl (9 M, 10 mL) and stirred for 5 minutes, then Ti_3AlC_2 (0.5 g) powder was slowly added and stirred at 35 ^oC for 24 h. Then, the pH of the washing supernatant reached 6, and the solid precipitate was added to DI water and sonicated for 1.0 hour under a stream of nitrogen. Using differential centrifugation (3500 rpm and 8000 rpm) for 1 h, the supernatant was collected as a Ti_3C_2 (MXenes) solution, and protected by nitrogen. Then, PEI of 5 mg mL^{-1} was added into the MXenes suspension and slowly stirred at room temperature for 1 h. Subsequently, the suspension was centrifuged, and the sediment was redispersed in DI water. After that, carboxylated g-C_3N_4 was synthesized according to the procedure reported previously.[52] Briefly, the preparation process of carboxylated g-C_3N_4 was introduced: bulk g-C_3N_4 was prepared in a tube furnace by heating melamine at 550 ^oC for 4 h with a slope of about 3 ^oC min^{-1} under air conditions. Then, 100 mg of g-C_3N_4 powder was ground, added to 100 mL of HNO_3 and refluxed for 24 h, and then the supernatant was separated and subjected to ultrasound for 16 h. The initially formed suspension was then centrifuged at about 10000 rmp and dispersed into a DI water. Then, g-C_3N_4 of 0.03 mg mL^{-1} was activated in EDC (400 mM) and NHS (100 mM) at 37 ^oC for 1 h and was centrifuged. Then, the MXenes nanosheets were added to the g-C_3N_4 solution and kept at room temperature for 1 h. Finally, the mixture was centrifuged at 6000 rpm and dispersed into aqueous solution.

Biosensor Fabrication. The Au electrode was successively polished with 0.05 μm Al_2O_3 powder following by washing with ethanol and DI water under sonication. After being dried with N_2, the Au electrode was activated in 0.5 M H_2SO_4 between -0.20 and 1.65 V (vs Ag/AgCl) before modification. It was immersed into the PBS (10 mM, pH 7.4) containing 500 μM cysteine terminated kemptide for 12 h in darkness at room temperature. After rinsing with PBS, the resulting electrode was treated with 1 mM MCH solution for 30 min to block the electrode. Then, the electrode was immersed in

PBS containing a desired amount of PKA and ATP in an incubator. Afterward, the resulting electrode was incubated in the solution containing g-C_3N_4-MXenes probes and left standing for 120 min at room temperature. Finally, the generated electrode was thoroughly washed with water to remove non-specificity g-C_3N_4-MXenes. The construction process is shown in Scheme 1.

Preparation of MCF-7 cell lysate. MCF-7 cells (1×10^5) were cultured in DMEM medium supplement at 37 °C under a humidified atmosphere containing 5% CO_2. The culture medium was replaced by serum-free medium, and the cells were further incubated for 4 h. Subsequently, MCF-7 cells were treated with Forskolin/IBMX solution (1:2 in molar ratio) for activating the intracellular PKA activity. After that, 2 mL lysis buffer were treated by the cultured cells for 5 min, then the cell lysates were centrifuged at 12,000 rpm. Finally, the resulting supernatants were stored at -80 °C for the subsequent experiments.

RESULTS AND DISCUSSION

Characterization of g-C_3N_4-MXenes Nanoprobes. The morphologies of g-C_3N_4 nanoparticles, MXenes and g-C_3N_4-MXenes nanocomplex were characterized by TEM (Figure 1A). g-C_3N_4 nanoparticles present the disk-like shape with the size of 100 nm (Figure 1A), and the prepared MXenes shows a typical sheet shape (Figure 1B). The MXenes were further characterized by AFM (Figure S1). The MXenes nanosheets show the thickness of ca. 1.2 nm, indicating that the as fabricated MXenes are single layer. Scheme 1A shows the synthesis processes of the g-C_3N_4-MXenes hybrids. MXenes was stripped from the MAX bulk material into single layer, and was assembled with PEI. After that, the g-C_3N_4 decorated MXenes nanohybrids were synthesized by the crosslink between the amino groups on PEI and the carboxyl groups on the acidified g-C_3N_4. After the conjugation of g-C_3N_4, lots of gray dots on the MXene were observed by the TEM (Figure 1C). The decoration of g-C_3N_4 on MXenes was also characterized by XRD, as shown in Figure 1D. The characteristic diffraction peak of (002) of g-C_3N_4 (curve a) in XRD patterns centering at 27.4° pertained to the obvious graphitic

interlayer stack. As a while, the diffraction peak of (100) at 13.1° is ascribed to tri-s-triazine units (curve b). After the conjugation, the typical diffraction peaks of both g-C_3N_4 and Ti_3C_2 can be observed from the g-C_3N_4-MXenes (curve c), indicating the formation of g-C_3N_4-MXenes hybrid.

Figure 1E shows the FT-IR spectra of MXenes (curve a), g-C_3N_4 (curve b), g-C_3N_4 -MXenes (curve c). The peaks of MXenes at 657 cm^{-1} and 1625 cm^{-1} correspond to the Ti-H bending vibration in MXenes. The peak at 804 cm^{-1} in curve b corresponds to the triazine bonds stretching vibration in g-C_3N_4. The peaks of the N-H (1537 cm^{-1}), C=O (1630 cm^{-1}) and Ti-H (658 cm^{-1}) can also be observed in that of g-C_3N_4-MXenes. Afterward, the carboxylated g-C_3N_4 NPs conjugated PEI-MXenes (g-C_3N_4-MXenes) was fabricated by amidation reaction between carboxyl groups on the carboxylated g-C_3N_4 NPs and amino groups on the surface of PEI. Zeta potentials were also conducted to demonstrate the generation of the g-C_3N_4 decorated MXenes. Figure 1F presents the zeta potentials changes of MXenes. The as prepared MXenes exhibited negative potential, and the potential change to positive after the adsorption of PEI. After the formation of g-C_3N_4-MXenes hybrid, the charges reduced owing the conjugation of negative charged g-C_3N_4. These results demonstrated the formation of g-C_3N_4 -MXenes, and were used in the following experiments.

ECL Behaviors of the g-C_3N_4-MXenes Nanoprobes. To investigate the ECL behaviors of g-C_3N_4-MXenes nanoprobes, various g-C_3N_4 NPs and g-C_3N_4-MXenes modified Au electrode were studied, respectively. As shown in Figure 2A, the bare gold electrode (curve a) almost has no ECL signal in PBS containing KCl and $K_2S_2O_8$. And g-C_3N_4 NPs modified Au electrode (curve b) also has no ECL signal in PBS containing KCl. In addition, there is nearly no ECL signa on the Ti_3C_2 MXenes modified Au electrode in the PBS with $S_2O_8^{2-}$ and KCl (curve c). However, a strong ECL emission response presented at the g-C_3N_4 NPs modified Au electrode in the PBS with the existence of $S_2O_8^{2-}$ and KCl (curve d), ascribing to the strong high-energy annihilation between the electrons injected into the conduction band of g-C3N4 by the anodic electrode and holes injected into the valence band of g-C3N4 by the electrogenerated g-C_3N_4 from $S_2O_8^{2-}$. Moreover, a sharper ECL emission was given by the g-C_3N_4-

MXenes modified Au electrode in presence of KCl and $S_2O_8^{2-}$ (curve e), which was about 7 times of that on the g-C_3N_4 modified Au electrode (curve d). These results suggest that the MXenes significantly enhance the ECL signal of g-C_3N_4-$K_2S_2O_8$ system which could be ascribed to its excellent conductivity and catalytic performance that can mediate over-injected electrons into g-C_3N_4 conduction band (CB) by transferring partial electrons to Ti_3C_2 MXene, and preventing g-C_3N_4 from being electrochemically degraded (Figure S2). In addition, the electrochemical behaviors of the modified electrodes were also studied. Figure 2B shows that the bare Au electrode (curve a) has an obvious reductive peak in PBS containing KCl and $K_2S_2O_8$ owing to the reduction of $K_2S_2O_8$. In addition, a weak reductive peak was observed on the g-C_3N_4 NPs modified gold electrode (curve b) in PBS, which may due to the injection of electrons into the g-C_3N_4 NPs layer.[52] When the g-C_3N_4 NPs modified Au electrode was scanned in the presence of KCl and $S_2O_8^{2-}$, a negative cathodic peak at -0.77 V (curve c) was presented, which was caused by the strong annihilation when the g-C_3N_4 NPs reduced into g-$C_3N_4^{\bullet-}$, and $SO_4^{\bullet-}$ was electrogenerated from $S_2O_8^{2-}$.[53] The reductive peak was shifted to -0.66 V (curve d) on the g-C_3N_4-MXenes modified Au electrode in PBS containing KCl and $K_2S_2O_8$, which could be ascribed to the electrocatalytic reduction of $S_2O_8^{2-}$ on MXenes that provided the reaction with affluent hole-donor ($SO_4^{\bullet-}$ free radical) toward g-C_3N_4 ECL reaction. These results indicate that MXenes can catalyze persulfate to provide more offer abundant $SO_4^{\bullet-}$ free radical, thus accelerating the reaction. Figure 2C shows the ECL responses of the g-C_3N_4 NPs and g-C_3N_4-MXenes modified Au electrodes. Both of them exhibited the ECL emission peaks at the same wavelength of 550 nm which came from the g-C_3N_4 that was oxidized to the excited state g-$C_3N_4^*$ while it fell to the ground state, and emitted light occurred. In addition, the ECL emission from the g-C_3N_4-MXenes modified Au electrodes were obviously much stronger than that of g-C_3N_4 modified electrode, which could be attributed to the excellent conductivity that facilitated the electron transfer on the electrode interface and large surface area of MXenes for more g-C_3N_4 bounded. Moreover, the g-C_3N_4-MXenes modified electrode exhibits excellent cyclic stability under the same potential conditions (Figure 2D), which could be ascribed to the

inhibitory action of MXenes toward the electrode passivation during the negative potential scanning like those of liquid metals and gold nanoparticles.[32,53] These facts indicate that the g-C_3N_4-MXenes can be excellent ECL nanoprobes for the fabrication of biosensor with high performances.

Construction of the Biosensor for Protein Kinases Analysis.

Scheme 1B presents the ECL biosensor for protein kinases detection based on the g-C_3N_4-MXenes nanoprobe. The cysteine-terminated kemptides were assembled on the Au electrode through the Au-S bond. Then, the kemptide/Au electrode was treated with MCH to block blank binding sites. In the presence of PKA and ATP, the hydroxy in the serine of kemptide was phosphorylated and conjugated with g-C_3N_4-MXenes nanocomposites by the chelation interaction between Ti defect sites on MXenes and phosphate groups. The plenty of Ti defect sites on MXenes provides more active sites for the highly efficient recognition of phosphorylated kemptide and the nanoprobes. Owing to the excellent conductivity and catalytic activity, large surface area of MXene, the ECL signal could be improved obviously by catalyzing the g-C_3N_4 ECL reaction with the coreactor of $S_2O_8^{2-}$ and promoting the electron transfer at the electrode interface. Hence, strong and stable ECL signal are obtained, which provides a sensitive tool for kinase activity evaluation.

Electrochemical Characterizations of the Biosensor. Electrochemical impedance spectroscopy (EIS), as an effective means, was adopted for monitoring the assembly processes of the modified electrodes by evaluating their charge transfer resistance (R_{et}), in which the diameter of the semicircle corresponded to the electron transfer resistance at the electrode interface.[54,55] As exhibited in Figure 3A, the bare Au electrode (curve a) exhibits a small R_{et}. After the immobilization of kemptide, the R_{et} of the electrode gradually increase (curve b), which is ascribed to the electron inert feature of kemptide that blocked the electron transfer. After kemptide is phosphorylated by PKA (curve c), the EIS of the resulting assembled layer shows a larger R_{et} since the hydroxide group of kemptide is replaced by phosphate group and hence increase the electrostatic repulsion between the negative charged phosphate groups and electroactive probes. After successful treatment of g-C_3N_4-MXenes, the R_{et} of the electrode gradually

decreased (curve d), which was ascribed to the excellent conductivity of MXene, indicating the successful construction of ECL biosensor. In addition, the surface coverage (θ_E) of kemptide on the electrode was calculated to be 83% according to the equation: θ_E kemptide = (1- R_{et}/ $R_{et}^{kemptide}$) ×100%, where R_{et} is the charge transfer resistance of the gold surface, and $R_{et}^{kemptide}$ is the corresponding resistance of kemptide modified gold surface.

ECL Behaviors of the Biosensor. In this design, the ECL signals from g-C_3N_4-MXenes nanoprobe are closely relevant to the phosphorylated kemptide on the electrode. The ECL behaviors of the biosensor was studied. As shown in Figure 3B, the ECL responses on the bare Au electrode (curve a), MCH/kemptide/Au (curve b), phosphorylated kemptide/MCH/Au (curve c) are nearly negligible. In the absence of MXenes, g-C_3N_4/phosphorylated kemptide/MCH/Au (curve d) shows a weak ECL signal, indicating that the non-specific adsorption of g-C_3N_4 could be neglected. In addition, the kemptide/MCH/Au in the absence of protein kinase also shows a negligible ECL response after treatment of g-C_3N_4-MXenes (curve e). As a while, the ECL signal of the g-C_3N_4-MXenes/phosphorylated kemptide/MCH/Au after the treatment of phosphorylation shows a much stronger ECL signal (curve f). The facts are attributed to the specific interaction between the Ti defect sites and the phosphor groups that g-C_3N_4-MXenes hybrid nanoprobes can specifically adsorbed onto the phosphorylated kemptide modified electrode. To confirm the facts, a series of control experiments were performed. Figure 3C shows the ECL behaviors of phosphorylated kemptide modified electrodes treated with g-C_3N_4-MXenes (curve a), g-C_3N_4 (curve b), and PEI-MXenes (curve c), respectively. It is obvious that the ECL signal from the g-C_3N_4-MXenes modified electrode with phosphorylated kemptide is significantly stronger than those on g-C_3N_4 and PEI-MXenes, indicating the highly efficient recognition and signal amplification of the g-C_3N_4-MXenes hybrid nanoprobes which can be applied for highly sensitive kinase activity analysis.

Optimization of the Detection Conditions. The phosphorylation times, probe incubation times and concentrations of ATP were crucial parameters for the detection of PKA. It is observed (Figure S3A) that the ECL signal reaches the maximum value

when the phosphorylation time is 90 min, and keep a steady state after that. As a result, the optimal phosphorylation time is 90 min. As can be seen from Figure S3B, the maximum intensity achieves at 120 min with increasing g-C_3N_4-MXenes probes incubation time. Therefore, the optimal time for g-C_3N_4-MXenes probes incubating on the phosphorylated kemptide is 120 min. In addition, the ECL intensity increased with the ATP concentration and then reached equilibrium at 80 μM (Figure S3C). After that, the increasing ATP concentration no longer enhances the ECL intensity. Thus, the optimal concentration of ATP is 80 μM.

Activity Determination of PKA. Under the optimal conditions, the activity of PKA of ECL biosensor was evaluated. The change of ECL signals under potential scanning at different concentrations of PKA (Figure 4A) shows that the ECL intensity is enhanced gradually with concentrations of PKA. There is a linear relationship between the ECL intensity and the log (C_{PKA}) in the range of 0.015 to 40 U mL^{-1}. The linear equation is I (the ECL intensity) = 676 log [C_{PKA}] − 726 with a correlation coefficient (R^2) of 0.96484 (n = 3), where I_{ECL} is the ECL intensity and *C* is the concentrations of kinase activity (Figure 4B). The LOD is calculated to be 1.0 mU/mL on basis of log (LOD) = 3θ/k (θ = the background standard deviation, k = 676), which shows excellent performance compared with the previous reports (Table S1). The promotion of the sensitivity benefits from the highly efficient recognition and the multiple ECL signal amplification of the g-C_3N_4-MXenes hybrid nanoprobes. These results demonstrate that the designed ECL biosensor of g-C_3N_4-MXenes could be applied for highly sensitive detection of PKA activity.

The proteins kinase plays an important role in regulating biological function. In this strategy, the ECL signal is not only associated with the concentration of proteins kinase but also relates to the level of proteins kinase expression. Thus, the selectivity of the biosensor was studied, for the detection of bovine serum albumin (BSA), hemoglobin and glucose oxidase (Figure S4A) with five times of the concentration of PKA. It is observed that PKA presents a higher ECL signal than that other enzymes. The fact indicates that the proposed ECL biosensor presents excellent selectivity toward PKA activity evaluation. Moreover, the stability of the designed biosensor was also

evaluated by assaying the PKA activity of 0.10 U mL^{-1}, and the ECL signal kept stable after 10 cycles and the RSD was 2.52% (Figure S4B), suggesting the excellent stability of the biosensor.

PKA Inhibition Evaluation and PKA Detection in Cell Lysates. To evaluate the potential application in the inhibition effects, the assays were carried out with kinase inhibitors at different concentrations. As shown in Figure 5A, the ECL intensity decreases with increasing concentration of ellagic acid, and then reaches a stable level, which indicates the inhibition effect of ellagic acid on the PKA activity. The half-maximal inhibition values (IC_{50}) of ellagic acid is calculated to be 3.87 μM, which is very close to the reported value.[56] In addition, the PKA activity evaluation was conducted in the presence of Tyrphostin AG 1478 (curve b) and EGCG (curve c) as shown in Figure 5A. The ECL signal exhibits negligible change with the variation of concentration of Tyrphostin AG 1478 and EGCG. These results clearly demonstrate that the ECL method afford a sensitive, rapid way in kinase inhibitors screening.

Protein kinase overexpression is associated with cell proliferation and tumor transformation. Therefore, under certain stimulation, the detection of PKA activity in cell lysates is necessary. MCF-7 cells were stimulated by the accelerators of Forskolin/IBMX and the inhibitors of ellagic acid, respectively. As shown in Figure 5B, the ECL response induces by the MCF-7 cell lysate increases with Forskolin/IBMX stimulation, demonstrating the PKA activity is activated. On the contrary, the cell lysate stimulated with ellagic acid exhibits the lowest PKA activity. As shown in Figure 5C**,** with increasing concentrations of Forskolin/IBMX, the ECL intensity increases and then reaches a stable level at 25 μM, which indicates the promoting effect of Forskolin on the PKA activity in MCF-7 cells lysates. The above facts clearly indicate that the proposed g-C_3N_4-MXenes based ECL biosensor has the potential for kinase analysis in cell samples, demonstrating the potential applications of the ECL biosensor for in vitro cell drugs screening and clinic diagnostics.

CONCLUSIONS

In summary, a novel all-in-one g-C_3N_4 NPs-modified MXenes hybrid nanoprobe was successfully used for the construction of ECL biosensor for PKA activity determination. The MXenes hybrid nanoprobe enriches the numerous of Ti active sites that can chelate to the phosphate groups on the phosphorylated kemptide. Moreover, the excellent conductivity and large surface of MXene can accommodate more g-C_3N_4 NPs and facilitate the electron transfer on the electrode interface and avoid the passivation of g-C_3N_4 NPs, affording the strong and stable ECL signal emission. The unique features integrating the highly efficient recognition and multiple signal amplification make the ECL biosensor for PKA activity detection with high sensitivity in the absence of metal ions or biorecognition units such as antibody or DNA linker. Moreover, the constructed biosensor was successfully used for the inhibitor screening and monitoring of the PKA activity in MCF-7 cell lysates. This method present great prospect in clinic diagnostic as well as life science research.

ACKNOWLEDGMENTS

This work was financially supported by National Key Research and Development Program of China (No.2016YFA0203101), National Natural Science Foundation of China (No. 21874080， 21974042, 21874042, 21622506, 21621003), the Scientific Research Fund of Hunan Provincial Education Department (18A010).

ASSOCIATED CONTENT

Supporting Information

The main content of the supporting information includes the figures for Ti_3C_2 MXenes characterization, interference experiments, sensor conditions' optimization and comparison of linear ranges and PKA detection limits by ECL detection methods.

Notes

The authors declare no competing financial interest.

REFERENCES

(1) Zaha, V. G.; Young, L. H. *Circ. Res.* **2012**, *111*, 800-814.

(2) Sebolt-Leopold, J. S.; Herrera, R. *Nat. Rev. Cancer.* **2004**, *4*, 937-947.

(3) Manning, G.; Whyte, D. B.; Martinez, R.; Hunter, T.; Sudarsanam, S. *Science* 2002, *298*, 1912−1934.

(4) Yan, Z.; Deng, P.; Liu, Y. *Int. J. Mol. Sci.* **2019**, *20*.

(5) Maqbool, M.; Mobashir, M.; Hoda, N. *Eur. J. Med. Chem.* **2016**, *107*, 63-81.

(6) Podolec, P. *Eur. Heart. J.* **2017**, *38*, 3190-3192.

(7) Kempf, C.; Tinguely, M.; Rushing, E. J. *Pathobiology* **2013**, *80*, 310-318.

(8) Wang, Z.; Sun, N.; He, Y.; Liu, Y.; Li, J. *Anal. Chem.* 2014, *86,* 6153−6159.

(9) Meng, F.-N.; Ying, Y.-L.; Yang, J.; Long, Y.-T. *Anal.Chem.* **2019**, *91*, 9910-9915.

(10) Ji, J.; Yang, H.; Liu, Y.; Chen, H.; Kong, J.; Liu, B. *Chem.Commun.* **2009**, 1508.

(11) Wang, C.-L.; Wei, L.-Y.; Yuan, C.-J.; Hwang, K. C. *Anal.Chem.* **2012**, *84*, 971-977.

(12) Jung, H.; Choi, Y.; Lee, D.; Seo, J. K.; Kee, J.-M. *Chem.Commun.* **2019**, *55*, 7482-7485.

(13) Shen, C.; Xia, X.; Hu, S.; Yang, M.; Wang, J. *Anal.Chem.* **2015**, *87*, 693-698.

(14) Manning, G.; Whyte, D. B.; Martinez, R.; Hunter, T.; Sudarsanam, S. *Science* 2002, *298*, 1912−1934.

(15) Zhang, N.; Gao, H.; Xu, C. H.; Cheng, Y.; Chen, H. Y.; Xu, J. J. *Anal. Chem.* **2019**, *91*, 12553-12559.

(16) Yang, L.; Fan, D.; Zhang, Y.; Ding, C.; Wu, D.; Wei, Q.; Ju, H. *Anal. Chem.* **2019**, *91*, 7145-7152.

(17) Lei, J.; Ju, H. *Chem. Soc. Rev.* **2012**, *41*, 2122-2134.

(18) Kannan, P.; Chen, J.; Su, F.; Guo, Z.; Huang, Y. *Anal.Chem.* **2019**, *91*, 14792-14802.

(19) Liu, Z.; Qi, W.; Xu, G. *Chem. Soc. Rev.* **2015**, *44*, 3117-3142.

(20) Liu, X.; Dong, M.; Qi, H.; Gao, Q.; Zhang, C. *Anal.Chem.* **2016**, *88*, 8720-8727.

(21) Yin, H.; Wang, M.; Li, B.; Yang, Z.; Zhou, Y.; Ai, S. *Biosens. Bioelectron.* **2015**,

63, 26-32.

(22) Xu, S.; Liu, Y.; Wang, T.; Li, J. *Anal.Chem.* **2010**, *82*, 9566-9572.

(23) Zhao, H.-F.; Liang, R.-P.; Wang, J.-W.; Qiu, J.-D. *Chem.Commun.* **2015**, *51*, 12669-12672.

(24) Wang, Z.; Yan, Z.; Sun, N.; Liu, Y. *Biosens. Bioelectron.* **2015**, *68*, 771-776.

(25) Yan, Z.; Wang, F.; Deng, P.; Wang, Y.; Cai, K.; Chen, Y.; Wang, Z.; Liu, Y. *Biosens. Bioelectron.* **2018**, *109*, 132-138.

(26) Yang, S. B.; Gong, Y. J.; Zhang, J. S.; Zhan, L.; Ma, L. L.; Fang, Z. Y.; Vajtai, R.; Wang, X. C.; Ajayan, P. M. *Adv. Mater.* 2013, *25*, 2452−2456.

(27) Cheng, Y.; Wang, L.; Song, Y.; Zhang, Y. *J. Mater. Chem. A.* **2019**, *7*, 15862-15870.

(28) Xu, B.; Zhu, M.; Zhang, W.; Zhen, X.; Pei, Z.; Xue, Q.; Zhi, C.; Shi, P. *Adv. Mater.* **2016**, *28*, 3333-3339.

(29) Naguib, M.; Mochalin, V. N.; Barsoum, M. W.; Gogotsi, Y. *Adv. Mater.* **2014**, *26*, 992-1005.

(30) Hong Ng, V. M.; Huang, H.; Zhou, K.; Lee, P. S.; Que, W.; Xu, J. Z.; Kong, L. B. *J. Mater. Chem. A.* **2017**, *5*, 3039-3068.

(31) Hantanasirisakul, K.; Gogotsi, Y. *Adv. Mater.* **2018**, *30*, e1804779.

(32) Zhang, Q.; Wang, F.; Zhang, H.; Zhang, Y.; Liu, M.; Liu, Y. *Anal. Chem.* **2018**, *90*, 12737-12744.

(33) Zhang, S.; Li, X.-Y.; Yang, W.; Tian, H.; Han, Z.; Ying, H.; Wang, G.; Han, W.-Q. *ACS Appl. Mater. Inter.* **2019**, *11*, 42086-42093.

(34) Zhang, J.; Zhao, Y.; Guo, X.; Chen, C.; Dong, C.-L.; Liu, R.-S.; Han, C.-P.; Li, Y.; Gogotsi, Y.; Wang, G. *Nature Catalysis* **2018**, *1*, 985-992.

(35) Tang, Y.; Yang, C.; Tian, Y.; Luo, Y.; Yin, X.; Que, W. *Nanoscale Advances* **2020**.

(36) Hart, J. L.; Hantanasirisakul, K.; Lang, A. C.; Anasori, B.; Pinto, D.; Pivak, Y.; van Omme, J. T.; May, S. J.; Gogotsi, Y.; Taheri, M. L. *Nat. Commun.* **2019**, *10*, 522.

(37) Li, P.; Zhu, J.; Handoko, A. D.; Zhang, R.; Wang, H.; Legut, D.; Wen, X.; Fu, Z.; Seh, Z. W.; Zhang, Q. *J. Mater. Chem. A.* **2018**, *6*, 4271-4278.

(38) Cheng, C.; Zhang, X.; Yang, Z.; Zhou, Z. *ACS Appl. Mater. Inter.* **2018**, *10*, 32903-

32912.

(39) Chen, H.; Handoko, A. D.; Xiao, J.; Feng, X.; Fan, Y.; Wang, T.; Legut, D.; Seh, Z. W.; Zhang, Q. *ACS Appl. Mater. Inter.* **2019**, *11*, 36571-36579.

(40) Attanayake, N. H.; Abeyweera, S. C.; Thenuwara, A. C.; Anasori, B.; Gogotsi, Y.; Sun, Y.; Strongin, D. R. *J. Mater. Chem. A.* **2018**, *6*, 16882-16889.

(41) Ghidiu, M.; Lukatskaya, M. R.; Zhao, M.-Q.; Gogotsi, Y.; Barsoum, M. W. *Nature* **2014**, *516*, 78-81.

(42) Zhu, Y.-P.; Lei, Y.; Ming, F.; Abou-Hamad, E.; Emwas, A.-H.; Hedhili, M. N.; Alshareef, H. N. *Nano Energy* **2019**, *65*, 104030.

(43) Luo, Y.; Chen, G.-F.; Ding, L.; Chen, X.; Ding, L.-X.; Wang, H. *Joule* **2019**, *3*, 279-289.

(44) Rakhi, R. B.; Nayak, P.; Xia, C.; Alshareef, H. N. *Sci. Rep-UK.* **2016**, *6*, 36422.

(45) Lorencova, L.; Bertok, T.; Filip, J.; Jerigova, M.; Velic, D.; Kasak, P.; Mahmoud, K. A.; Tkac, J. *Sensor. Actuat. B-Chem.* **2018**, *263*, 360-368.

(46) Zhang, H.; Wang, Z.; Zhang, Q.; Wang, F.; Liu, Y. *Biosens. Bioelectron.* **2019**, *124-125*, 184-190.

(47) Lu, Z.; Wei, Y.; Deng, J.; Ding, L.; Li, Z.-K.; Wang, H. *ACS Nano* **2019**, *13*, 10535-10544.

(48) Ciou, J.-H.; Li, S.; Lee, P. S. *Small* **2019**, *15*, 1903281.

(49) Dai, C.; Chen, Y.; Jing, X.; Xiang, L.; Yang, D.; Lin, H.; Liu, Z.; Han, X.; Wu, R. *ACS Nano* **2017**, *11*, 12696-12712.

(50) Han, X.; Huang, J.; Lin, H.; Wang, Z.; Li, P.; Chen, Y. *Adv. Healthc. Mater.* **2018**, *7*, 1701394.

(51) Ghidiu, M.; Halim, J.; Kota, S.; Bish, D.; Gogotsi, Y.; Barsoum, M. W. *Chem. Mater.* **2016**, *28*, 3507-3514.

(52) Lichan, C.; Danjun, H.; Shuyan, R.; Tongqing, D.; Yuwu, C.; Guonan, C. *Nanoscale* **2013**, *5*, 225−230.

(53) Jin, Y.; Kang, Q.; Guo, X.; Zhang, B.; Shen, D.; Zou, G. *Ana.l Chem.* **2018**, *90*, 12930-12936.

(54) Chen, L.; Zeng, X.; Si, P.; Chen, Y.; Chi, Y.; Kim, D. H.; Chen, G. *Anal. Chem.*

2014, *86*, 4188-4195.

(55) Jiang, J.; Lin, X.; Ding, D.; Diao, G. *RSC Adv.* **2018**, *8*, 19369-19380.

(56) Wang, W.; Liu, Y.; Shi, T.; Sun, J.; Mo, F.; Liu, X. *Anal. Chem.* **2020**, *92*, 1598-1604.

Legends

Scheme 1. Schematic illustration of the fabrication procedures of (A) g-C_3N_4-MXenes nanoprobe and (B) the g-C_3N_4-MXenes based biosensor and signal amplification strategy for PKA activity analysis.

Figure 1. TEM images of (A) g-C_3N_4 NPs, (B) MXenes and (C) g-C_3N_4-MXenes. (D) XRD patterns of carboxylated g-C_3N_4 (a), Ti_3C_2 MXenes (b) and g-C_3N_4-MXenes (c). (E) FT-IR spectra of MXenes (a), carboxylated g-C_3N_4 (b), g-C_3N_4-MXenes (c). (F) Zeta potentials of MXenes (a) PEI-MXenes (b) carboxylated g-C_3N_4 (c) g-C_3N_4-MXenes (d).

Figure 2. (A) ECL intensity−potential behavior obtained at bare Au electrode in PBS containing 20 mM $K_2S_2O_8$ (curve a), g-C_3N_4 modified Au electrode in PBS (curve b), Ti_3C_2 MXenes modified Au electrode (curve c), g-C_3N_4 modified Au electrode (curve d) and g-C_3N_4-MXenes modified Au electrode (curve e) in PBS containing 20 mM $K_2S_2O_8$. (B) cyclic voltammograms of (curve a) bare Au electrode in PBS containing 20 mM $K_2S_2O_8$, the g-C_3N_4 NPs modified gold electrode in the PBS solution (curve b) without and (curve c) with 20 mM $K_2S_2O_8$, and (curve d) g-C_3N_4-MXenes modified Au electrode in PBS containing 20 mM $K_2S_2O_8$. (C) ECL spectra of the g-C_3N_4-MXenes (black) and g-C_3N_4 (red) modified Au electrode in PBS containing 20 mM $K_2S_2O_8$. (D) The ECL-time curves of g-C_3N_4 -MXenes modified Au electrode in PBS containing 20 mM $K_2S_2O_8$. The voltage of PMT is 400 V.

Figure 3. (A) Electrochemical impedance spectra of the bare Au electrode (a), MCH/kemptide/Au (b), phosphorylated kemptide/MCH/Au (c), g-C_3N_4-MXenes/phosphorylated kemptide/MCH/Au (d) recorded in 5 mM $[Fe(CN)_6]^{4-/3-}$ containing 0.1 M KCl (pH 7.4). The impedance spectra frequency was 0.1-100 kHz. (B) The ECL intensity-potential curves of the bare Au electrode (a), MCH/kemptide/Au (b), phosphorylated kemptide/MCH/Au (c), g-C_3N_4/phosphorylated

kemptide/MCH/Au (d), g-C_3N_4-MXenes/MCH/kemptide/Au (e), g-C_3N_4-MXenes/phosphorylated kemptide/MCH/Au (f) at the concentrations of PKA of 0.10 U mL^{-1}. (C) The ECL intensity response of the phosphorylated kemptide Au electrode with the treatment of g-C_3N_4-MXenes probes (a), g-C_3N_4 probes (b), PEI-MXenes probes (c). The scan rates were 100 mV s^{-1}. All ECL experiments were carried out in PBS containing 20 mM $K_2S_2O_8$ and 0.1 M KCl. The voltage of PMT was set as 600 V.

Figure 4. (A) The ECL intensity-time curves in the PBS containing 20 mM $K_2S_2O_8$ and 0.1M KCl and PKA with different concentrations from 0.015-40 U mL^{-1}. (B) The ECL intensity at different PKA concentrations from 0.015 to 40 U mL^{-1}. The inset is the linear relationship between ECL intensity and PKA concentrations. The scan rate is 100 mV s^{-1}. The voltage is maintained at 600 V. The potential goes from -1.2 to 0 V. The error bars represent the standard deviation of three measurements.

Figure 5. (A) The ECL intensity of different concentrations of ellagic acid (a) and Tyrphostin AG 1478 (b) and EGCG (c). The concentrations of PKA and ATP are 0.20 U mL^{-1} and 80 μM, respectively. (B) The ECL intensity of the PKA expression in MCF-7 cells lysates stimulated by Forskolin, ellagic acid and PBS buffer (control), respectively. The error bars represent the standard deviation of three measurements. (C) The dependence of the ECL intensity on different concentrations of Forskolin and IBMX. The scan rate is 100 mV s^{-1}. The voltage is maintained at 600 V. The potential goes from -1.2 to 0 V. The error bars represent the standard deviation of three measurements.

Scheme 1

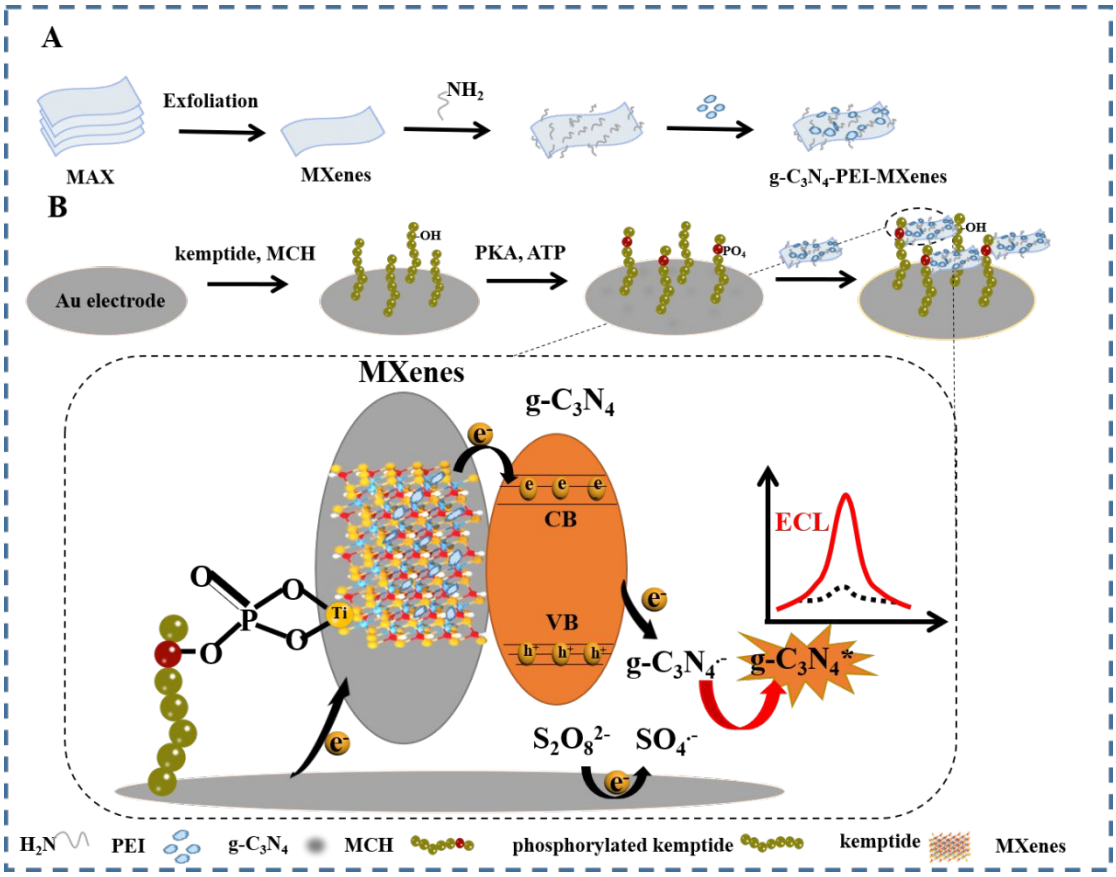
A
Exfoliation
NH2
MAX
MXenes
g-C3N4-PEI-MXenes
B
kemptide, MCH
PKA, ATP
Au electrode
OH
PO4
MXenes
g-C3N4
CB
VB
ECL
Ti
g-C3N4*
S2O8 2-
SO4 -
H2N
PEI
g-C3N4
MCH
phosphorylated kemptide
kemptide
MXenes

Figure 1

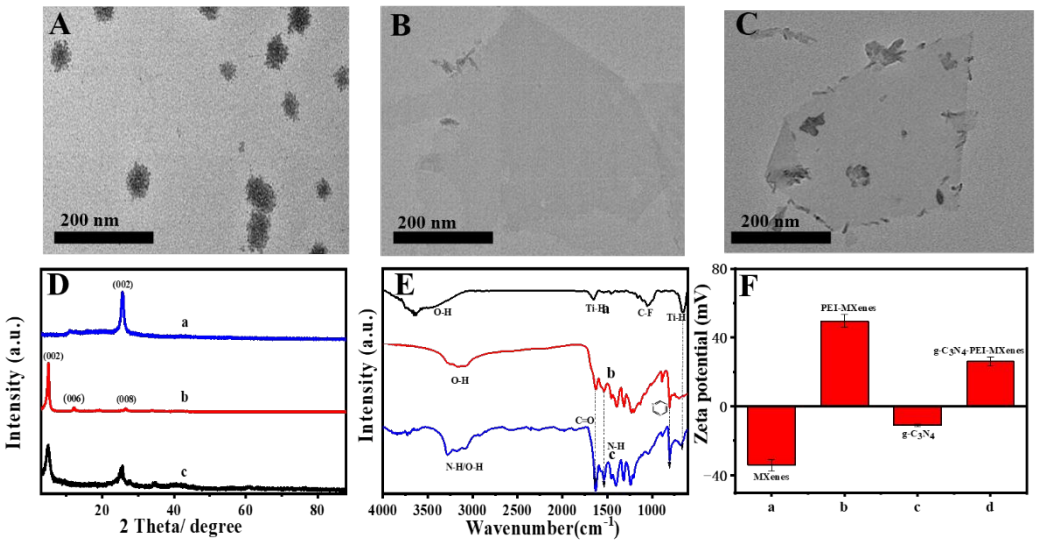
A
200 nm
B
200 nm
C
200 nm
D
(002)
a
(002)
(006)
(008)
b
c
Intensity (a.u.)
20
40
60
80
2 Theta/ degree
E
O-H
Ti-H
C-F
Ti-H
O-H
b
C=O
N-H
c
N-H/O-H
Intensity (a.u.)
4000
3500
3000
2500
2000
1500
1000
Wavenumber(cm-1)
F
80
40
0
−40
Zeta potential (mV)
PEI-MXenes
g-C3N4-PEI-MXenes
g-C3N4
MXenes
a
b
c
d

Figure 2

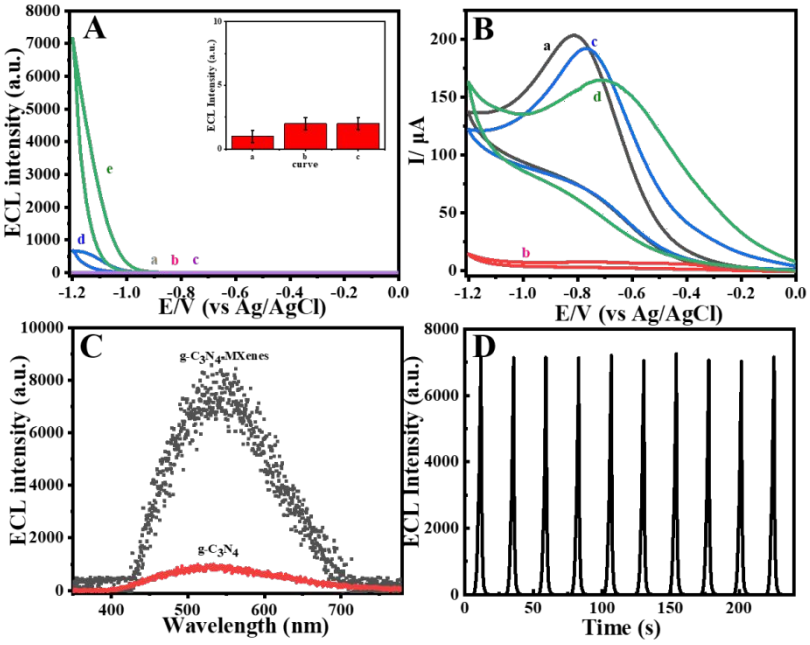
A
ECL intensity (a.u.)
E/V (vs Ag/AgCl)
ECL Intensity (a.u.)
curve
a b c d e
B
I/ μA
E/V (vs Ag/AgCl)
a c d b
C
g-C3N4-MXenes
g-C3N4
ECL intensity (a.u.)
Wavelength (nm)
D
ECL Intensity (a.u.)
Time (s)

Figure 3

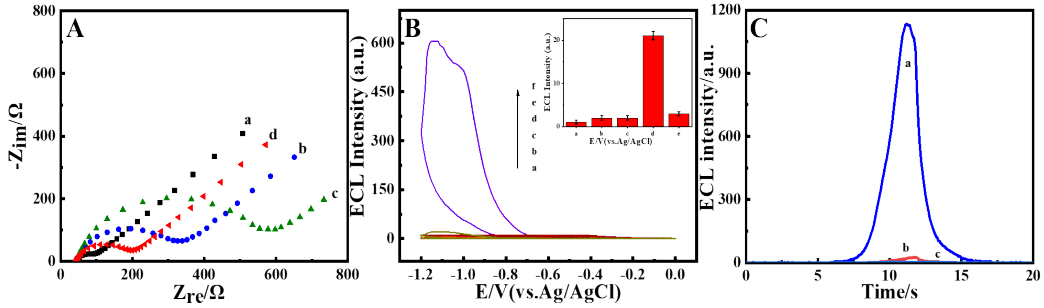
A
-Zim/Ω
Zre/Ω
a
b
c
d
B
ECL Intensity (a.u.)
E/V(vs.Ag/AgCl)
C
ECL intensity/a.u.
Time/s

Figure 4

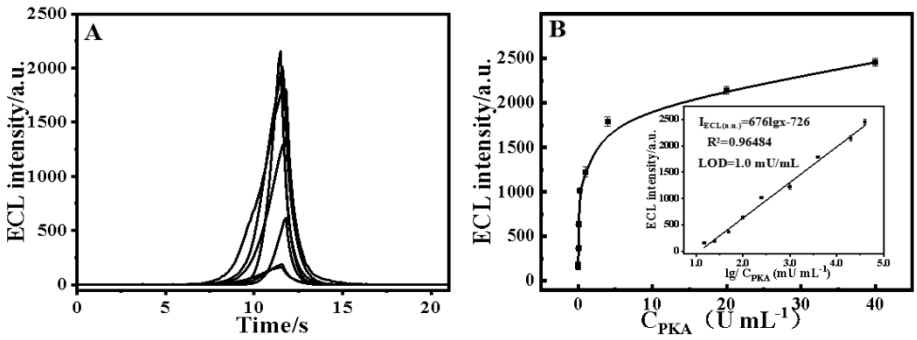
A
ECL intensity/a.u.
Time/s
B
ECL intensity/a.u.
C_{PKA} (U mL^{-1})
$I_{ECL(a.u.)}$=676lgx-726
R^2=0.96484
LOD=1.0 mU/mL
lg/ C_{PKA} (mU mL^{-1})

Figure 5

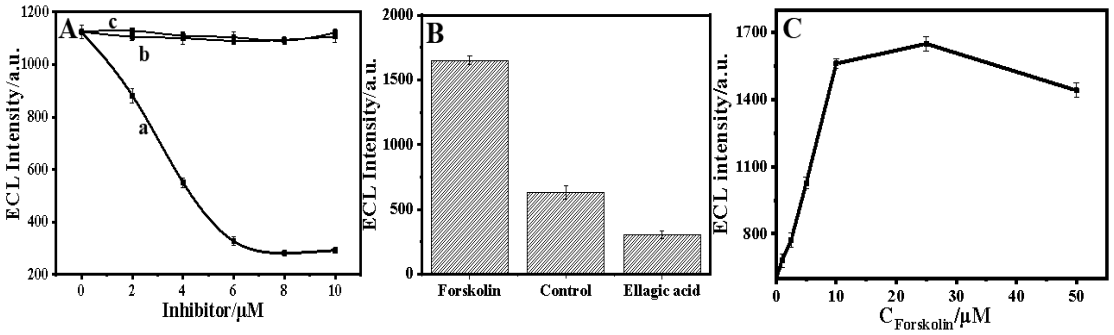
A
c
b
a
ECL Intensity/a.u.
Inhibitor/μM
B
ECL Intensity/a.u.
Forskolin
Control
Ellagic acid
C
ECL intensity/a.u.
C Forskolin/μM

For Table of Contents Only